Table 3
Average changes in CBF and MBR after intravenous administration of ET-1.

	Baseline levels	30 min	60 min
CBF (mL/min/100 g)	41.6 ± 10.2	41.9 ± 9.8 (1.02 ± 0.15)	39.4 ± 10.5 (0.95 ± 0.16)
MBR	4.1 ± 0.8	3.9 ± 1.0 (0.95 ± 0.08)	3.9 ± 0.7 (0.95 ± 0.20)

Data are expressed as mean ± SD for 6 rabbits. No significant difference was found. CBF/MBR changes to baseline levels were shown in parentheses.

3.3. *Effects of individuality and treatment*

Randomized block ANOVA revealed that there were wide ranges of distribution of differences for the basal blood flow measurement and that animals' individuality had significant effects on MBR and CBF (Table 1). Distributions of differences for the time-course changes were relatively narrow. Although the time-course changes in MBR and CBF during ET-1 treatment were not significant, those during CO_2 treatment were significant by repeated measure analysis (Table 1).

Average and individual changes in CBF after treatments are shown in Tables 2 and 3 and Fig. 4, respectively. CBF had a tendency of increasing after CO_2 inhalation (CBF was increased in 6 cases out of 9). ET-1 administration decreased CBF in 5 cases out of 6 though the effect was not significant because CBF was markedly increased in just one case. Representative hydrogen density curve charts are shown in Fig. 5. Average changes in MBR after treatments are shown in Tables 2 and 3. Typical examples of 2-dimensional color-coded MBR maps are shown in Fig. 6.

4. Discussion

This report is the first to verify the correlation of MBR, a new index obtained by CCD-equipped LSFG, with CBF obtained by the hydrogen gas clearance method in the ONH. A significant and positive correlation between the absolute values of CBF and MBR at baseline, as well as their relative changes, was found in the current study. This result suggests that MBR may correlate with CBF and also change with CBF, as an index of blood flow in the ONH, linearly. Since a similar experiment cannot be performed in humans, the present study provides important basal data for the measurement of MBR in humans, though these data cannot be applied directly to humans because of their many histophysiological differences with rabbits.

A power analysis (Correlation: point biserial model) by G* Power software (v. 3.1.3) showed that total sample size of 9 is needed under the condition of effect size of 0.7, error probability (α) of 0.05 and power ($1 - \beta$) of 0.8. Therefore, the sample sizes of 14 and 39 in the current study would be sufficient statistically.

In the present study, inhalation of CO_2 or intravenous administration of ET-1 altered CBF obtained by the hydrogen gas clearance method in rabbit ONH. These results are, at least partly, consistent with previous reports (Sugiyama et al., 1995, 1996). The relative values of CBF and MBR to the initial levels were in the range of 0.74–1.27 and 0.76–1.35, respectively. A significant and positive correlation was also found between the relative changes in CBF and MBR values induced by CO_2 inhalation and ET-1 injection. This correlation suggests that changes in MBR may indicate those in CBF in the ONH. These results appear similar to a previous report (Sugiyama et al., 1996). Though the r value in this study (0.67) was obviously different from that in the previous paper (0.92), the comparison of r values from different experiments does not seem fair since they can be affected by many factors.

In the current study, the r value for the correlation between the absolute values of MBR and CBF was 0.73; this was relatively large and comparable to that between the relative values during CO_2 inhalation and ET-1 injection. This result indicates quantifiability of absolute values of MBR at least under a certain condition. On the other hand, the randomized block ANOVA in the current study revealed significant effects of the individuality of animals on basal values of CBF and MBR. Therefore, care must be taken in interpreting absolute values across individuals, even though the absolute values of MBR were significantly correlated with CBF. In general, measurement results obtained with apparatus that employ lasers are affected by the degree of absorption or reflection of the laser beam in the specific tissue. Particularly in humans, careful interpretation is needed due to relatively large topographical or color differences of the ONH induced by individuality or diseases, which affect absorption and reflection. Actually, we have data on individual variation in MBRs of young normal volunteers; MBRs in the temporal rim were measured in the range of 6.3–13.8 (mean ± SD = 10.6 ± 2.5, n = 9). In addition, MBRs in the nasal

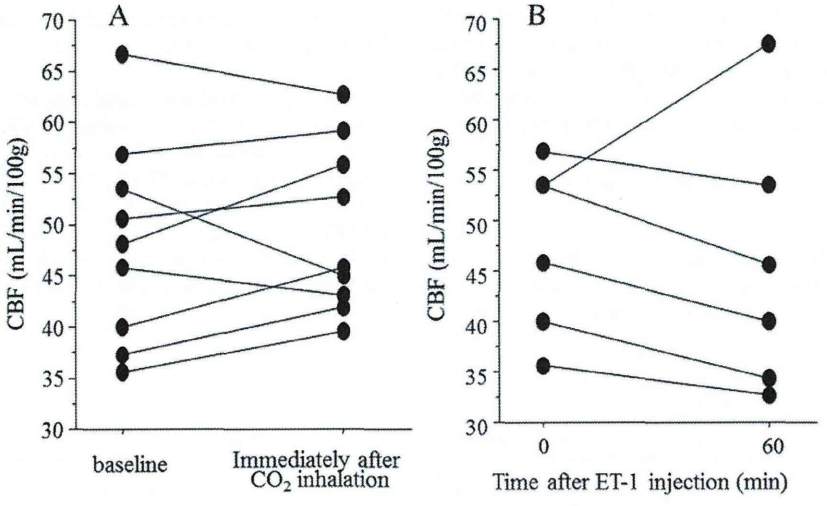

Fig. 4. Individual changes in CBF after 5-min inhalation of 10% CO_2 (A) and administration of 10^{-10} mol/kg ET-1 (B). CBF was increased in 6 cases out of 9, and decreased in 5 cases out of 6 in A and B, respectively.

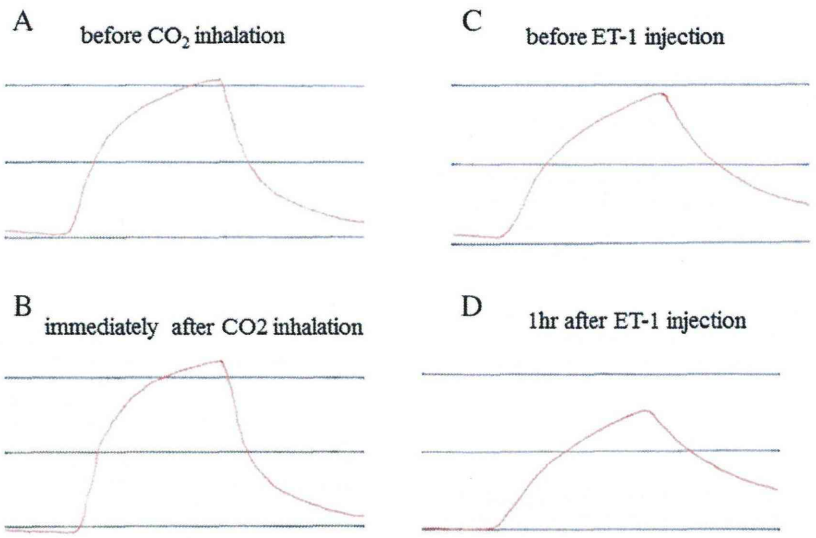

Fig. 5. Representative examples of the hydrogen gas clearance curve. A and B: before and immediately after 5-min inhalation of 10% CO_2 in the same rabbit (A is the same as Fig. 1A). CBF values were 65.3 and 77.6 mL/min/100 g, respectively. C and D: before and 1 h after administration of 10^{-10} mol/kg ET-1 in another same rabbit. CBF values were 40.3 and 32.8 mL/min/100 g, respectively.

rim of them were measured as 17.8 ± 3.9, which are much different from those in the temporal rim. Therefore, the relatively wide range of ONH blood flow in the present study might be due to an individual difference as well as a regional difference.

As a problematic issue for the LSFG apparatus, the zero-offset for MBR was rather large (around 2.5) in the current study. We actually obtained 6.1 and 1.9 as mean values of MBR ($n = 2$) at the same spot of ONH just before and shortly after a rabbit was euthanized (the hydrogen gas clearance method cannot be available while it is dead because inhalation is impossible then) in the additional experiment. This result (mean value of MBR was 1.9 when blood flow was stopped in dead rabbits) is almost consistent with the zero-offset of approximately 2.5. In addition, since a range of baseline values of MBR was 3.5–6.0, the ratio of the highest to the lowest (6.0/3.5) was smaller than those by the hydrogen gas clearance method (83.5/32.4). Taken together, there seems to be a room for more

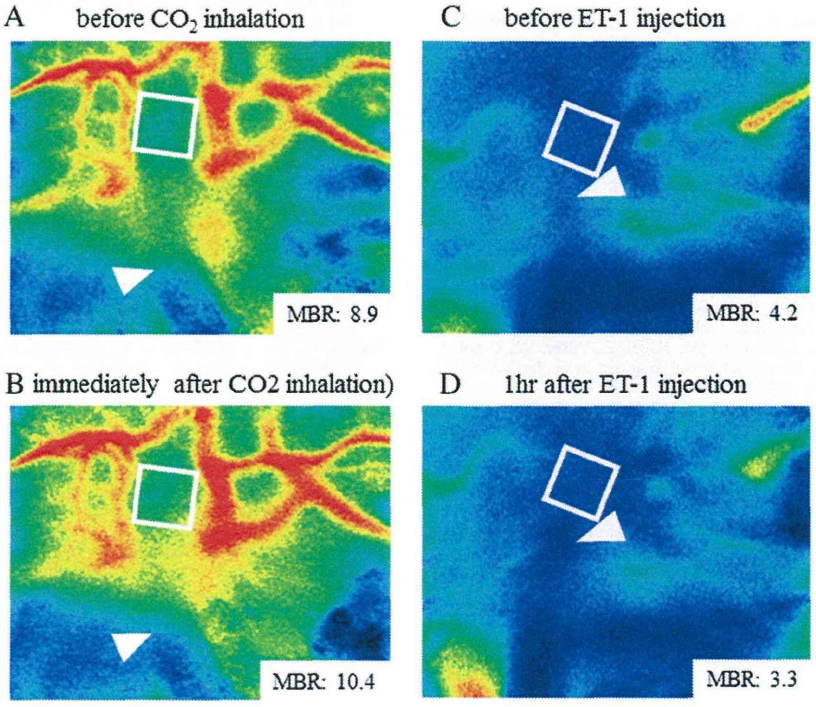

Fig. 6. Representative examples of color-coded MBR maps obtained by LSFG. A and B: before and immediately after 5-min inhalation of 10% CO_2 in the same rabbit. C and D: before and 1 h after administration of 10^{-10} mol/kg ET-1 in another rabbit. Arrowheads indicate the tips of electrodes for the hydrogen gas clearance method, and white squares indicate the areas analyzed by LSFG.

adequate calibration of MBR values. While these results (a relatively large zero-offset and a smaller relative change in MBR) were only for the animal model in the current study. Further investigation using other animals should also be needed in the future for validation of quantifiability of measurement of ONH microcirculation by LSFG.

Many agents have been reported to alter ocular blood flow (Araie and Mayama, 2011; Shimazawa et al., 1999; Sugiyama and Azuma, 1995; Sugiyama et al., 2010, 2011; Tokushige et al., 2011; Waki et al., 2001). Since the present study revealed that MBR may correlate with tissue blood flow in the ONH, LSFG-NAVI™ will likely provide new relevant information concerning the ONH blood flow in glaucoma and support in verifying whether increasing ONH blood flow could be a promising strategy for glaucoma management.

5. Conclusions

Our results suggest that MBR obtained by CCD-equipped LSFG may correlate with CBF and also change with CBF, as an index of blood flow in the ONH, linearly.

Financial disclosure

H. Takahashi and H. Tokushige are employees of Senju Pharmaceutical Co., Ltd. The other authors have no financial disclosures.

Acknowledgments

The authors thank Y.T. for her technical support and kindest encouragement, Mr. Mitsunori Waki for his technical advice and valuable discussions, and Dr. Tomoyuki Wada for his advice concerning statistics and his encouragement.

References

Aizawa, N., Yokoyama, Y., Chiba, N., Omodaka, K., Yasuda, M., Otomo, T., Nakamura, M., Fuse, N., Nakazawa, T., 2011. Reproducibility of retinal circulation measurements obtained using laser speckle flowgraphy-NAVI in patients with glaucoma. Clin. Ophthalmol. 5, 1171–1176.

Araie, M., Mayama, C., 2011. Use of calcium channel blockers for glaucoma. Prog. Retin. Eye Res. 30, 54–71.

Aukland, K., Bower, B.F., Berliner, R.W., 1964. Measurement of local blood flow with hydrogen gas. Circ. Res. 14, 164–187.

Caprioli, J., Coleman, A.L., 2010. Blood pressure, perfusion pressure, and glaucoma. Am. J. Ophthalmol. 149, 704–712.

Csete, K., Vezekényi, Z., Dóczi, T., Papp, J.G., Bodosi, M., Barzó, P., 2004. Comparison of regional vasomotor responses to acetazolamide and CO_2 in rabbit cerebrum and cerebellum, measured by a hydrogen clearance method. Acta Physiol. Scand. 182, 287–294.

Ernest, J.T., 1976. Optic disc blood flow. Trans. Ophthalmol. Soc. U.K. 96, 348–351.

Garhofer, G., Bek, T., Boehm, A.G., Gherghel, D., Grunwald, J., Jeppesen, P., Kergoat, H., Kotliar, K., Lanzl, I., Lovasik, J.V., Nagel, E., Vilser, W., Orgul, S., Schmetterer, L., 2010. Use of the retinal vessel analyzer in ocular blood flow research. Acta Ophthalmol. 88, 717–722.

Grieshaber, M.C., Mozaffarieh, M., Flammer, J., 2007. What is the link between vascular dysregulation and glaucoma? Surv. Ophthalmol. 52 (Suppl. 2), S144–S154.

Harris, A., Kagemann, L., Ehrlich, R., Rospigliosi, C., Moore, D., Siesky, B., 2008a. Measuring and interpreting ocular blood flow and metabolism in glaucoma. Can. J. Ophthalmol. 43, 328–336.

Harris, A., Werne, A., Cantor, L.B., 2008b. Vascular abnormalities in glaucoma: from population-based studies to the clinic? Am. J. Ophthalmol. 145, 595–597.

Konishi, N., Tokimoto, Y., Kohra, K., Fujii, H., 2002. New laser speckle flowgraphy system using CCD camera. Opt. Rev. 9, 163–169.

Logan, J.F., Rankin, S.J., Jackson, A.J., 2004. Retinal blood flow measurements and neuroretinal rim damage in glaucoma. Br. J. Ophthalmol. 88, 1049–1054.

Moore, D., Harris, A., Wudunn, D., Kheradiya, N., Siesky, B., 2008. Dysfunctional regulation of ocular blood flow: a risk factor for glaucoma? Clin. Ophthalmol. 2, 849–861.

Nagahara, M., Tamaki, Y., Araie, M., Fujii, H., 1999. Real-time blood velocity measurements in human retinal vein using the laser speckle phenomenon. Jpn. J. Ophthalmol. 43, 186–195.

Pemp, B., Georgopoulos, M., Vass, C., Fuchsjager-Mayrl, G., Luksch, A., Rainer, G., Schmetterer, L., 2009. Diurnal fluctuation of ocular blood flow parameters in patients with primary open-angle glaucoma and healthy subjects. Br. J. Ophthalmol. 93, 486–491.

Riva, C.E., Geiser, M., Petrig, B.L., 2010. Ocular blood flow assessment using continuous laser doppler flowmetry. Acta Ophthalmol. 88, 622–629.

Shimazawa, M., Sugiyama, T., Azuma, I., Araie, M., Iwakura, Y., Watari, M., Sakai, T., Hara, H., 1999. Effect of lomerizine, a new Ca^{2+}channel blocker, on the microcirculation in the optic nerve head in conscious rabbits: a study using a laser speckle technique. Exp. Eye Res. 69, 185–193.

Srinivasan, V.J., Atochin, D.N., Radhakrishnan, H., Jiang, J.Y., Ruvinskaya, S., Wu, W., Barry, S., Cable, A.E., Ayata, C., Huang, P.L., Boas, D.A., 2011. Optical coherence tomography for the quantitative study of cerebrovascular physiology. J. Cereb. Blood Flow Metab. 31, 1339–1345.

Stalmans, I., Vandewalle, E., Anderson, D.R., Costa, V.P., Frenkel, R.E., Garhofer, G., Grunwald, J., Gugleta, K., Harris, A., Hudson, C., Januleviciene, I., Kagemann, L., Kergoat, H., Lovasik, J.V., Lanzl, I., Martinez, A., Nguyen, Q.D., Plange, N., Reitsamer, H.A., Sehi, M., Siesky, B., Zeitz, O., Orgul, S., Schmetterer, L., 2011. Use of colour doppler imaging in ocular blood flow research. Acta Ophthalmol. 89, e609–630.

Sugiyama, T., Araie, M., Riva, C.E., Schmetterer, L., Orgul, S., 2010. Use of laser speckle flowgraphy in ocular blood flow research. Acta Ophthalmol. 88, 723–729.

Sugiyama, T., Azuma, I., 1995. Effect of UF-021 on optic nerve head circulation in rabbits. Jpn. J. Ophthalmol. 39, 124–129.

Sugiyama, T., Moriya, S., Oku, H., Azuma, I., 1995. Association of endothelin-1 with normal tension glaucoma: clinical and fundamental studies. Surv. Ophthalmol. 39 (Suppl. 1), S49–S56.

Sugiyama, T., Shibata, M., Kajiura, S., Okuno, T., Tonari, M., Oku, H., Ikeda, T., 2011. Effects of fasudil, a rho-associated protein kinase inhibitor, on optic nerve head blood flow in rabbits. Invest. Ophthalmol. Vis. Sci. 52, 64–69.

Sugiyama, T., Utsumi, T., Azuma, I., Fujii, H., 1996. Measurement of optic nerve head circulation: comparison of laser speckle and hydrogen clearance methods. Jpn. J. Ophthalmol. 40, 339–343.

Takayama, J., Tomidokoro, A., Ishii, K., Tamaki, Y., Fukaya, Y., Hosokawa, T., Araie, M., 2003. Time course of the change in optic nerve head circulation after an acute increase in intraocular pressure. Invest. Ophthalmol. Vis. Sci. 44, 3977–3985.

Tamaki, Y., Araie, M., Fukaya, Y., Nagahara, M., Imamura, A., Honda, M., Obata, R., Tomita, K., 2003. Effects of lomerizine, a calcium channel antagonist, on retinal and optic nerve head circulation in rabbits and humans. Invest. Ophthalmol. Vis. Sci. 44, 4864–4871.

Tamaki, Y., Araie, M., Kawamoto, E., Eguchi, S., Fujii, H., 1995. Non-contact, two-dimensional measurement of tissue circulation in choroid and optic nerve head using laser speckle phenomenon. Exp. Eye Res. 60, 373–383.

Tamaki, Y., Araie, M., Kawamoto, E., Eguchi, S., Fujii, H., 1994. Noncontact, two-dimensional measurement of retinal microcirculation using laser speckle phenomenon. Invest. Ophthalmol. Vis. Sci. 35, 3825–3834.

Tamaki, Y., Araie, M., Tomita, K., Tomidokoro, A., 1996. Time change of nicardipine effect on choroidal circulation in rabbit eyes. Curr. Eye Res. 15, 543–548.

Tokushige, H., Waki, M., Takayama, Y., Tanihara, H., 2011. Effects of Y-39983, a selective rho-associated protein kinase inhibitor, on blood flow in optic nerve head in rabbits and axonal regeneration of retinal ganglion cells in rats. Curr. Eye Res. 36, 964–970.

Tomidokoro, A., Araie, M., Tamaki, Y., Tomita, K., 1998. In vivo measurement of iridial circulation using laser speckle phenomenon. Invest. Ophthalmol. Vis. Sci. 39, 364–371.

Tomita, K., Araie, M., Tamaki, Y., Nagahara, M., Sugiyama, T., 1999. Effects of nilvadipine, a calcium antagonist, on rabbit ocular circulation and optic nerve head circulation in NTG subjects. Invest. Ophthalmol. Vis. Sci. 40, 1144–1151.

Waki, M., Sugiyama, T., Watanabe, N., Ogawa, T., Shirahase, H., Azuma, I., 2001. Effect of topically applied iganidipine dihydrochloride, a novel calcium antagonist, on optic nerve head circulation in rabbits. Jpn. J. Ophthalmol. 45, 76–83.

Watanabe, G., Fujii, H., Kishi, S., 2008. Imaging of choroidal hemodynamics in eyes with polypoidal choroidal vasculopathy using laser speckle phenomenon. Jpn. J. Ophthalmol. 52, 175–181.

Yamazaki, Y., Drance, S.M., 1997. The relationship between progression of visual field defects and retrobulbar circulation in patients with glaucoma. Am. J. Ophthalmol. 124, 287–295.

The American Journal of Pathology, Vol. 181, No. 1, July 2012

http://dx.doi.org/10.1016/j.ajpath.2012.03.022

Cell Injury, Repair, Aging, and Apoptosis

The Regulatory Roles of Apoptosis-Inducing Factor in the Formation and Regression Processes of Ocular Neovascularization

Toshio Hisatomi,*†‡ Shintaro Nakao,*† Yusuke Murakami,*† Kousuke Noda,* Toru Nakazawa,* Shoji Notomi,† Edward Connolly,* Haicheng She,* Lama Almulki,* Yasuhiro Ito,* Demetrios G. Vavvas,* Tatsuro Ishibashi,† and Joan W. Miller*

From the Angiogenesis Laboratory, Massachusetts Eye and Ear Infirmary, Department of Ophthalmology, Harvard Medical School, Boston, Massachusetts; the Department of Ophthalmology,† Graduate School of Medical Sciences, Kyushu University, Fukuoka, Japan; and the Clinical Research Institute,‡ Kyushu Medical Center, Fukuoka, Japan*

The role of apoptosis in the formation and regression of neovascularization is largely hypothesized, although the detailed mechanism remains unclear. Inflammatory cells and endothelial cells both participate and interact during neovascularization. During the early stage, these cells may migrate into an angiogenic site and form a pro-angiogenic microenvironment. Some angiogenic vessels appear to regress, whereas some vessels mature and remain. The control mechanisms of these processes, however, remain unknown. Previously, we reported that the prevention of mitochondrial apoptosis contributed to cellular survival via the prevention of the release of pro-apoptotic factors, such as apoptosis-inducing factor (AIF) and cytochrome *c*. In this study, we investigated the regulatory role of cellular apoptosis in angiogenesis using two models of ocular neovascularization: laser injury choroidal neovascularization and VEGF-induced corneal neovascularization in AIF-deficient mice. Averting apoptosis in AIF-deficient mice decreased apoptosis of leukocytes and endothelial cells compared to wild-type mice and resulted in the persistence of these cells at angiogenic sites *in vitro* and *in vivo*. Consequently, AIF deficiency expanded neovascularization and diminished vessel regression in these two models. We also observed that peritoneal macrophages from AIF-deficient mice showed anti-apoptotic survival compared to wild-type mice under conditions of starvation. Our data suggest that AIF-related apoptosis plays an important role in neovascularization and that mitochondria-regulated apoptosis could offer a new target for the treatment of pathological angiogenesis. *(Am J Pathol 2012, 181:53–61; http://dx.doi.org/10.1016/j.ajpath.2012.03.022)*

The mitochondrial apoptosis pathways are important mechanisms of cell death.[1] Mitochondria contain pro-apoptotic factors such as cytochrome *c* and apoptosis-inducing factor (AIF) in their intermembrane space. Furthermore, mitochondrial outer membrane permeabilization is a critical event during apoptosis, representing the "point of no return" of the lethal process. Cytochrome *c* is released from mitochondria on mitochondrial outer membrane permeabilization and binds to cytosolic apoptotic protease activating factor-1 to induce its dimerization and a conformational change.[2] Apoptotic protease activating factor-1 then oligomerizes into apoptosomes that recruit and activate caspase-9 followed by serial activation of apoptosis-execution molecules.[3,4] Mitochondrial outer membrane permeabilization, however, may cause cell death even if caspases are inhibited[5] and a broad caspase inhibitor (z-VAD-fmk) fails to block apoptosis in retinal neurons.[6] AIF is a caspase-independent apoptogenic factor and is normally confined to the mitochondrial intermembrane space.[7] Most cell death in vertebrates proceeds via the mitochondrial pathway of apoptosis, especially in mammalian cells.[8,9] During

Supported by an Alcon Research Award (J.W.M.), Japan Eye Bank Association (T.H.), a Bausch & Lomb Vitreoretinal Fellowship (T.N.), and National Eye Institute Grant EY014104 (Massachusetts Eye and Ear Infirmary Core Grant).

Accepted for publication March 15, 2012.

T.H., S.N., and Y.M. contributed equally to this work.

Address reprint requests to Joan W. Miller, M.D., Massachusetts Eye and Ear Infirmary, 243 Charles St., Boston, MA 02114, or Tatsuro Ishibashi, M.D., Ph.D., Department of Ophthalmology, Graduate School of Medical Sciences, Kyushu University, 3-1-1 Maidashi Higashi-ku, Fukuoka, 812-8582, Japan. E-mail: Joan_Miller@meei.harvard.edu or ishi@eye.med.kyushu-u.ac.jp.

apoptosis, AIF translocates to the cytosol and then to the nucleus where it triggers peripheral chromatin condensation and interacts with cyclophilin A to generate a DNase complex, which is responsible for the so-called "large-scale" DNA degradation to fragments of approximately 50 kbp.[10] AIF is strongly conserved among mammalian species (>95% amino acid identity between mouse and human) and bears a highly significant homology with flavoprotein oxidoreductases from all eukaryotic and prokaryotic kingdoms in its C-terminal portion.[7] Because AIF, a central player in mitochondrial apoptotic pathways is essential in the developmental process, AIF knockout mice die *in utero*.[11] Based on these findings, it is reasonable to speculate that AIF may be a phylogenetically old major mediator participating in various aspects of the apoptotic process. Because we originally reported AIF translocation in mammalian cells *in vivo* in retinal cell death,[6,9,12–16] the translocation of AIF has been reported in neurodegeneration[17,18] and retinal degeneration.[19] The contribution of apoptosis, especially phylogenetically old major factors (ie, AIF), however, has remained elusive in the field of neovascularization.

Choroidal neovascularization (CNV) is a pathological process involving the formation of new blood vessels from choroidal vasculature through Bruch's membrane breaks. CNV is associated with a variety of ocular diseases, including age-related macular degeneration (AMD), myopia, histoplasmosis, angioid streaks, tumors, and traumatic and idiopathic conditions, all of which often cause severe visual loss via retinal degeneration. CNV could be induced by focally increased inflammatory and proangiogenic factors, and/or by a decrease of anti-angiogenic factors. Various clinical, as well as experimental, studies have shown that vascular endothelial growth factor (VEGF)-A could be the most important factor for CNV.[20] Recent observations in age-related macular degeneration patients with VEGF-A inhibition strongly support the importance in CNV. In CNV, macrophages may be major sources of VEGF-A, which would enhance vascular leakage, as well as angiogenesis via vascular endothelial growth factor receptor (VEGFR)-2.[21] Macrophage also expresses VEGFR-1 and VEGF-A that may induce macrophage infiltration. Thus, VEGF is an inflammatory cytokine targeting both leukocytes and endothelial cells. Various studies have shown attachment of mural cells is important for the vascular stability that is dependent on angiopoietin/Tie system and VEGF.[22] Tie2 is known to play a direct role in pericyte recruitment and Tie2-knockout blood vessels that lack mural cells.[23] The loss of periendothelial cells in the mutants is secondary to endothelial cell apoptosis.[24]

The efficient clearance of excessive inflammatory cells and neovascular endothelial cells from the pathological sites may be essential for restoration of tissue homeostasis.[13] The regulation of apoptosis in angiogenesis-related cells, including leukocytes and endothelial cells, may occur in various disorders. The detailed mechanism, however, remains unclear.[25] In this study, we focused on the roles of a major proapoptotic molecule, AIF in the formation and regression of neovascularization.

Materials and Methods

Experimental Animals

All animal procedures were performed in accordance with the statement of the Association for Research in Vision and Ophthalmology and the protocol approved by the Animal Care Committee of Massachusetts Eye and Ear Infirmary. The AIF mutant mice (B6CBACa Aw-J/A-Aifm1Hq/J, stock number 000501; Jackson Laboratory, Bar Harbor, ME) and wild type (WT) from the colony were purchased from the Jackson Laboratory and bred in our laboratory. Adult male mice (8 weeks of age) were used for the following experiments.

Laser Injury-Induced Choroidal Neovascularization

Mice were anesthetized with ketamine (100 mg/kg) and xylazine (10 mg/kg). Pupils were dilated with 5.0% phenylephrine and 0.8% tropicamide. CNV was induced with a 532 nm laser (Oculight GLx, Iridex, Mountain View, CA) as previously described.[20,26–31] Four laser spots (150 mW, 100 msec, 50 μm settings) were placed in each eye using a slit-lamp delivery system and a cover glass as a contact lens (n = 16 for each time point and strain). Production of a bubble at the time of laser confirmed the rupture of the Bruch's membrane. The vessels were stained with fluorescein isothiocyanate-dextran. The eyes were enucleated at 2, 4, and 12 weeks after laser injury and fixed in 4% paraformaldehyde for 3 hours. The anterior segment and retina were removed from the eyecup. Approximately four to six relaxing radial incisions were made, and the remaining retinal pigment epithelial-choroidal-scleral complex was flat mounted and coverslipped. Pictures of the choroidal flat mounts were taken, and Openlab software version 5 (Improvision, Boston, MA) was used to measure the hyperfluorescent areas corresponding to the CNV lesions. The average size of the CNV lesions was then determined and used for the evaluation.

Bone Marrow Transplantation

To characterize the angiogenic roles of infiltrating macrophages, we produced chimera green fluorescent protein (GFP) mice, by a previously described method.[13,32] Briefly, we used the transgenic mouse as a cell source for enhanced GFP (EGFP)-positive bone marrow cells. The host mice took 1,4-butanediol dimethanesulfonate, Busulfan 4 × 25 mg/kg on 4 consecutive days followed by bone marrow transplantation (BMT) to deplete stem cells in the host and consequently allow for high levels of long-term, donor-type engraftment. A successful bone marrow transplantation was confirmed by the identification of GFP-positive cells in the blood at 2 and 4 weeks after BMT. The WT and AIF-deficient mice took BMT from EGFP transgenic mice and laser injury 4 weeks after BMT (n = 10, each group). The eyes were harvested and examined 2 weeks after laser injury, as previously described. To visualize EGFP-positive macrophage in the CNV, the vessels were stained with rhodamine-conjugated concanavalin A.

Corneal Micropocket Assay in Mice

Mice were anesthetized with ketamine (100 mg/kg) and xylazine (10 mg/kg). Poly 2-hydroxyethyl methacrylate pellets (0.3 μL, P3932; Sigma-Aldrich, St. Louis, MO) containing 200 ng VEGF-A (293-VE; R&D Systems, Minneapolis, MN) were prepared and implanted into the corneas. VEGF-A pellets were positioned at approximately 1 mm distant to the corneal limbus. After implantation, bacitracin ophthalmic ointment (E. Fougera & Co., Melville, NY) was applied to each eye to prevent infection. At 6 days (n = 6, each group), 10 days (n = 8), 14 days (n = 10), 28 days (n = 8), 56 days (n = 10), 84 days (n = 5), and 140 days (n = 3) after implantation, digital images of the corneal vessels were obtained and recorded using OpenLab software version (Improvision Inc., Lexington, MA) with standardized illumination and contrast. The quantitative analysis of neovascularization in the mouse corneas was performed using Scion Image software (version 4.0.2; Scion Corp., Frederick, MD).

TUNEL Assay

TUNEL and quantification of TUNEL$^+$ cells were performed as previously described,[6] using the ApopTag Fluorescein *in Situ* Apoptosis Detection Kit (Chemicon/Millipore, Bedford, MA). The center of the choroidal and corneal neovascularization was photographed, and the number of TUNEL$^+$ cells in the microscopic field was counted in a masked fashion. The results are presented as the mean ± SD.

Immunohistochemistry

The eyes were harvested and snap-frozen in optimal cutting temperature compound (Sakura Finetechnical). Sections (10 μm) were prepared, air dried, and fixed in ice-cold acetone for 10 minutes. The sections were blocked with 3% nonfat dried milk bovine working solution (M7409; Sigma-Aldrich) and stained with a macrophage marker, anti-mouse CD11b (1:50, BD Pharmingen, San Diego, CA) or an endothelial marker, anti-mouse CD31 mAb (1:50; BD Pharmingen), a myeloid lineage marker, CD45 (1:100, BD Pharmingen), VEGF, TNF-α (1:100, Santa Cruz Biotechnology, Santa Cruz, CA), basic fibroblast growth factor, IL-1β (Abcam, Cambridge, MA), and rabbit anti-AIF (1:50, R&D Systems).[33] After an overnight incubation, sections were washed and stained for 40 minutes with Alexa Fluor488 goat anti-rat IgG (20 μg/mL, A11006; Invitrogen). The specimens were observed with a fluorescent microscope and confocal microscope (Nikon, Tokyo, Japan).

Transmission Electron Microscopy

The eyes were enucleated and the posterior segments were fixed in 2.5% glutaraldehyde and 2% paraformaldehyde in 0.1 mol/L cacodylate buffer with 0.08 mol/L $CaCl_2$ at 4°C. The specimens were postfixed for 1.5 hours in 2% aqueous OsO_4, dehydrated in ethanol and water, and embedded in Epon (Electron Microscopy Sciences, Hatfield, PA). Ultrathin sections were cut from blocks and stained with saturated, aqueous uranyl acetate and Sato's lead stain. The specimens were observed with a Hitachi H-7650 electron microscope.

Fluorescein Angiography in CNV Model

Fluorescein angiography was performed by an operator masked to the genetic identity of the animal, with a commercial camera and imaging system (TRC 50 VT camera and IMAGEnet 1.53 system; Topcon, Paramus, NJ), at 2 weeks after laser photocoagulation (WT mice; n = 12, AIF-deficient mice; n = 12). The photographs were captured with a 20-dimensional lens in contact with the fundus camera lens, after intraperitoneal injection of 0.1 mL of 1% fluorescein sodium (Akorn, Decatur, IL). Two masked retina specialists evaluated the fluorescein angiograms at a single sitting. Lesions were graded on an ordinal scale based on the spatial and temporal evolution of fluorescein leakage as follows: grade 0 (nonleaky): no leakage, faint hyperfluorescence, or mottled fluorescence without leakage; grade1 (questionable leakage): hyperfluorescent lesion without progressive increase in size or intensity; grade 2A (leaky): hyperfluorescence increasing in intensity but not in size, no definite leakage; grade 2B (pathologically significant leakage): hyperfluorescence increasing in intensity and in size, definite leakage.[34]

Macrophage Culture from AIF-Deficient Mice

Briefly, peritoneal macrophages were collected by a previously described method.[14,35,36] Peritoneal macrophages were stimulated by injecting Thioglycollate medium into the mouse peritoneal space and collected by washing peritoneal space with 5 mL PBS. Cell density was adjusted to 3.5×10^4 cells each well of an 8-well chamber (Nunc, Thermo Fisher Scientific, Rochester, NY) with Dulbecco's modified Eagle's medium supplemented with 10% fetal bovine serum. We counted the number of TUNEL$^+$ apoptotic macrophages in the culture before and after starvation. For starvation, cells were cultured in Dulbecco's modified Eagle's medium without fetal bovine serum supplement and incubated for 24 hours. The number of TUNEL$^+$ apoptotic macrophages was counted in 10 random fields per well in a masked fashion using ImageJ software version 1.38x (NIH, Bethesda, MD) in Harlequin (Hq) and WT mice. Values are given as the mean ± SEM of 10 replicate wells.

Statistical Analysis

The data from the TUNEL and *in vitro* survival assays were analyzed with the Scheffé post hoc test using StatView 4.11J software for Macintosh (Abacus Concepts Inc., Berkeley, CA). Significance level was set at $P < 0.05$ and $P < 0.01$. The data represent mean ± SD, except for primary culture results.

Results

Nuclear AIF Translocation in TUNEL$^+$ Apoptotic Cells in the Mouse Choroidal Neovascularization

Laser injury-induced neovascular tissue formation from the choroid beneath the retina in 2 weeks in the WT mouse (Figure 1A). TUNEL$^+$ apoptotic cells were ob-

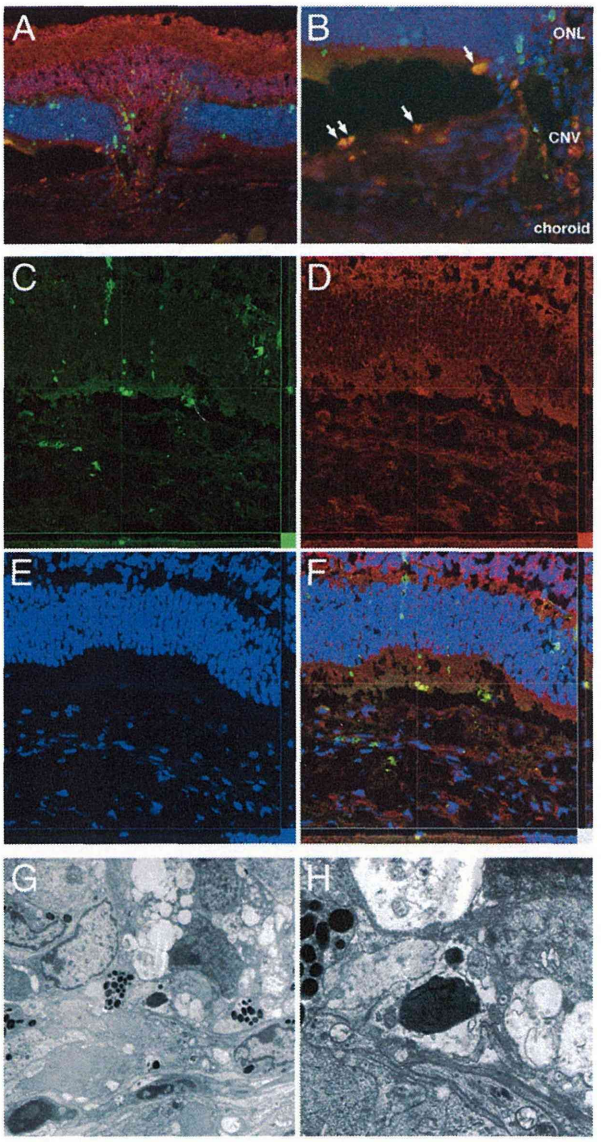

Figure 1. A: Apoptotic cell death and mitochondrio-nuclear translocation of AIF in choroidal neovascularization (CNV). The CNV developed from choroidal tissue into the subretinal space in the WT mouse. **B:** Abundant TUNEL$^+$ cells are observed in the CNV (green), and these cells also showed nuclear accumulation of AIF (red). In contrast, diffuse weak staining of AIF is observed in the cytosol of the nonapoptotic normal cells. **C–F:** Confocal microscopy also confirms co-localization of TUNEL (**C**) and AIF (**D**) in high resolution images. Nuclei are stained blue (**E**); merge is also shown (**F**). **G** and **H:** The electron microscopy shows the morphological characteristics of cellular apoptosis, namely chromatin condensation, cellular shrinkage, and apoptotic body formation in the CNV. Original magnification: ×200 (**A**); ×400 (**B–F**); ×750 (**G**) and ×2500 (**H**). ONL, outer nuclear layer.

served in the retina, subretinal space, and choroidal neovascularization. Nuclear translocation (accumulation) of AIF was abundantly observed in TUNEL$^+$ apoptotic cells in the subretinal space and the choroid (Figure 1B). In contrast, AIF is diffusely noted in the cytosol of the nonapoptotic normal cells. Confocal microscopy also confirmed co-localization of TUNEL and AIF in high resolution images (Figure 1, C–F). The electron microscopy showed the morphological characteristics of cellular apoptosis, namely *chromatin condensation, cellular shrinkage, and apoptotic* body formation (Figure 1, G and H).

AIF Deficiency Promotes CNV Expansion and Retards Regression

Hq mice exhibit an X chromosome-linked ataxia due to the progressive degeneration of terminally differentiated cerebellar neurons.[37,38] The Hq mutation has been identified as a proviral insertion in the apoptosis-inducing factor (*Aif*) gene (alias programmed cell death 8, *Pdcd8*), causing approximately an 80% reduction in AIF expression.[38] In contrast to Aif knockout mice, which die *in utero*,[11] Hq mice are born at normal Mendelian ratios and are healthy until the age of 3 months.

Laser-induced CNV in AIF-deficient mice led to lesions 1.7-fold larger than WT 2 weeks after laser (Figure 2, A–C). CNV also continues to grow in size in Hq mice to 4 weeks after laser, in contrast to WT mice (Figure 2C). CNV typically regresses rapidly in WT mice, but persists in Hq mice to 12 weeks. To test the regulatory roles of infiltrating macrophage in the CNV progression, we transplanted bone marrow cells from EGFP transgenic wt mice into WT and AIF-deficient mice 4 weeks before the laser injury (Figure 2, D

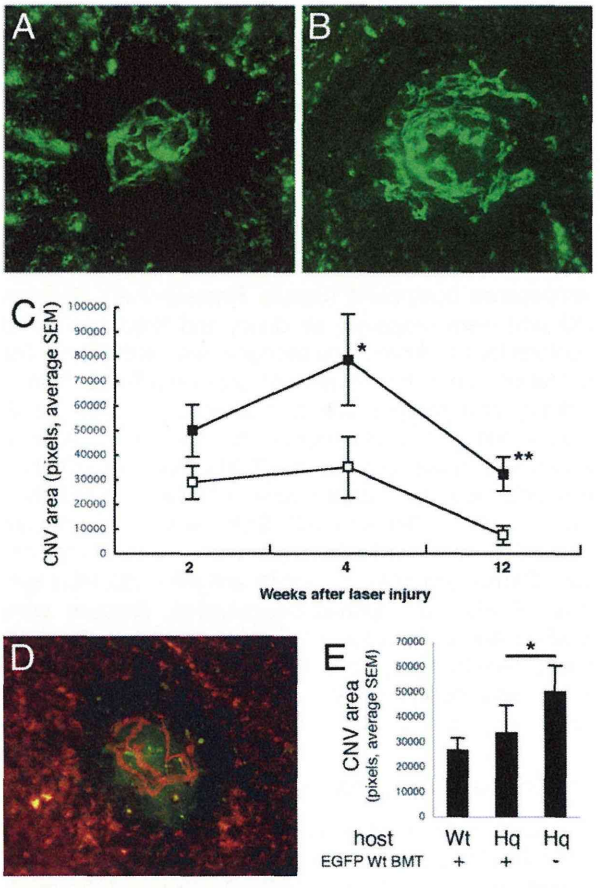

Figure 2. Choroidal neovascularization observed by choroidal flat mount. CNV is visualized with fluorescent injection and analyzed with analysis software. AIF-deficient mice (**B**) induce larger CNV formation than normal WT mice (**A**). **C:** Even after 12 weeks AIF-deficient mice (black box) show persistent CNV, whereas WT mice (white box) show regression of formed CNV. **D:** The EGFP-positive WT macrophages reconstructed from transplanted bone marrow migrate in the CNV stained with rhodamine conjugated concanavalin A. **E:** The CNV size increased in AIF-deficient mice compared to WT mice; conversely, CNV size was decreased in AIF-deficient mice with WT bone marrow transplantation. $^*P < 0.05$, $^{**}P < 0.01$. Hq, Harlequin.

and E). The EGFP-positive WT macrophages reconstructed from transplanted bone marrow migrated in the CNV (Figure 2D). The CNV size increased in AIF-deficient mice compared to WT mice, whereas the size was decreased in reverse in the AIF-deficient mice with WT bone marrow transplantation (Figure 2E). These experiments support that AIF deficiency resulted in enlarged CNV, which continued to grow and exhibited less regression relative to WT mice.

AIF Deficiency Decreases Apoptosis of Infiltrating Macrophages and Neovascular Endothelial Cells in CNV

Vertical histological sections also showed a large area of CNV in Hq mice in contrast to WT mice (Figure 3A). A large number of CD45-positive myeloid lineage cells migrated in the laser injury area and accumulated in the CNV. CD11b-positive macrophages were also present in CNV lesions (Figure 3B). In WT mice, TUNEL$^+$ apoptotic cells were abundant among CD11b(+) macrophages and CD31(+) endothelial cells. AIF-deficient mice, however, showed fewer TUNEL$^+$ apoptotic cells in the CNV. To test the roles of CD11b-positive macrophages, immunohistochemistry of CD11b and four major angiogenic or inflammatory factors, namely VEGF, TNF-α, basic fibroblast growth factor, and IL-1β, was examined in the CNV (Figure 3C). These four factors were expressed in CD11b positive macrophages. VEGF was strongly expressed in neovascular tissue, especially in the macrophages. These data suggest that AIF deficiency enhanced macrophage accumulation and angiogenic factor expression in the CNV.

AIF Deficiency Promotes CNV Leakage on Fluorescein Angiography

CNV leakage can be graded by fluorescein angiography, and in the clinical settting CNV leakage seems to correlate with CNV activity. AIF-deficient mice showed a trend toward a greater number of large, leaky, grade-2B lesions (denoting clinical significant leakage) than WT mice 2 weeks after laser (Figure 4).

AIF Deficiency Promotes Expansion of the Corneal Neovascularization and Retards Regression

Laser injury-induced choroidal neovascularization captures many of the important features of human conditions (ie, age-related macular degeneration), although this model includes various biological responses, such as thermal burn, tissue destruction, apoptosis and necrosis of retinal pigment epithelial cells, choroidal melanocytes, photoreceptors, or disruption of Bruch's membrane, and so forth. To clarify the role of AIF in VEGF-A–dependent angiogenesis, we used a simpler corneal pocket assay to induce angiogenesis in the corneas with AIF-deficient mice and WT mice. VEGF-A was implanted into these mice and the time course of VEGF-A–induced angiogenesis was followed until day 140. On day 6 after VEGF-A stimulation, the angiogenic

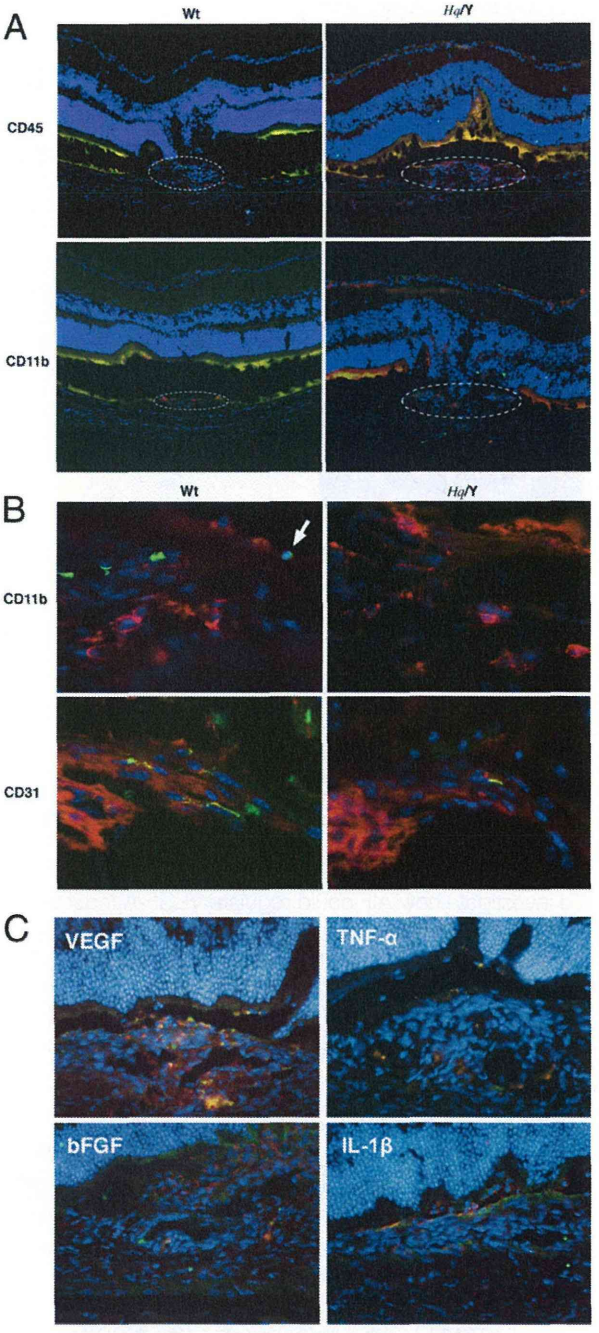

Figure 3. Immunohistochemistry for inflammatory and endothelial cells in CNV, which is observed at the laser injury site. A larger number of myeloid lineage cells (CD45) and macrophages (CD11b) migrate into CNV in apoptosis-inducing factor (AIF)-deficient mice compared to WT mice (**A**). TUNEL$^+$ inflammatory and endothelial cells are abundant in WT mice compared to AIF-deficient mice (**A**, **B**). **C:** Immunohistochemistry of CD11b and four major angiogenic or inflammatory factors (VEGF, TNF-α, bFGF, and IL-1β) were examined in the CNV. These four factors are expressed in CD11b-positive macrophages. VEGF is strongly expressed in neovascular tissue; however, it is especially expressed in the macrophages. AIF-deficiency enhances macrophage accumulation and angiogenic factor expression in the CNV. bFGF, basic fibroblast growth factor; Hq/Y, harlequin hemizygous male mice.

area in AIF-deficient mice was similar with WT mice, but by day 10 AIF-deficient mice showed a significantly greater area of corneal neovascularization than WT mice (Figure 5). The peak of the corneal neovascularization shifted from day

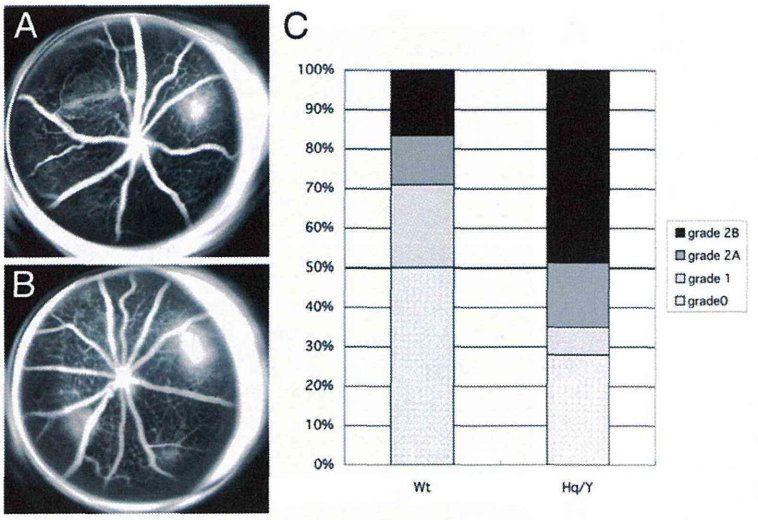

Figure 4. Fluorescein angiography of the laser-induced CNV. Compared to WT mice (**A**), AIF-deficient mice (**B**) developed larger CNV formation and more severe leakage. **C:** Lesions were graded on an ordinal scale based on the spatial and temporal evolution of fluorescein leakage as follows: grade 0 (nonleaky): no leakage, faint hyperfluorescence, or mottled fluorescence without leakage; grade 1 (questionable leakage): hyperfluorescent lesion without progressive increase in size or intensity; grade 2A (leaky): hyperfluorescence increasing in intensity but not in size; no definite leakage; grade 2B (pathologically significant leakage): hyperfluorescence increasing in intensity and in size; definite leakage. Hq/Y, harlequin hemizygous male mice.

28 in WT mice to day 56 in AIF-deficient mice. These data suggest that AIF may regulate VEGF-A-dependent angiogenesis at later stages of the process rather than the earlier step of angiogenic sprouting.

AIF Deficiency Decreases Apoptosis of Infiltrating Macrophages and Neovascular Endothelial Cells in VEGF-A-Induced Corneal Neovascularization

To investigate how AIF could regulate VEGF-A-induced angiogenesis, we hypothesized that cellular apoptosis by AIF could regulate the angiogenesis and checked apoptotic cells in VEGF-A-implanted AIF-deficient and WT mice with TUNEL staining. Immunostaining showed abundant infiltrated inflammatory cells (CD11b) and migrated neovascular endothelial cells (CD31) in AIF-deficient mice compared to WT mice (Figure 6A). Less TUNEL$^+$ cells in AIF-deficient mice could be observed than in WT mice at day 6 and at day 14 after VEGF-A implantation (Figure 6B). More TUNEL$^+$ apoptotic cells are noted on day 6 (early) than on day 14 (late) in WT mice. In contrast, more apoptotic cells are observed on day 14 (late) in AIF-deficient mice. AIF deficiency retarded cellular apoptosis in corneal neovascularization. These data suggest AIF could be important for cellular apoptosis during VEGF-A-induced angiogenesis.

Peritoneal Macrophages Are Resistant to Apoptosis in AIF-Deficient Mice

AIF deficiency promoted choroidal and corneal neovascularization, as well as accumulation of inflammatory cells (ie, CD45, 11b positive cells) at the local sites. To

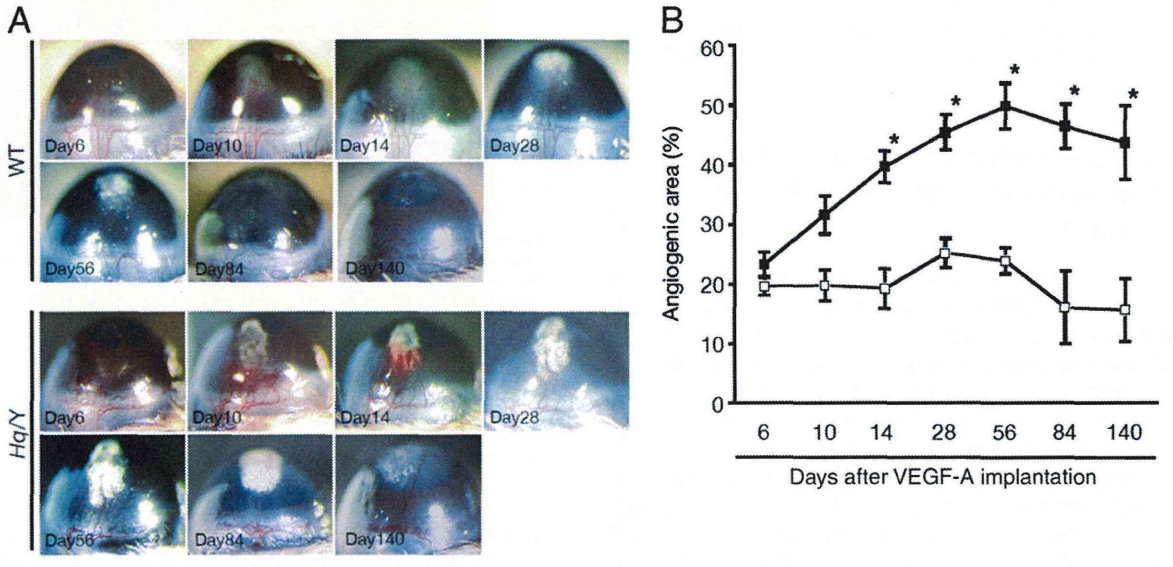

Figure 5. A: VEGF-induced corneal neovascularization by corneal micropocket assay. **B:** Pellets were implanted in the cornea, and the quantitative analysis of neovascularization in the mouse corneas was performed using image software. AIF-deficient mice (black box) develop larger neovascularization than WT mice (white box). The regression of the formed neovascularization is retarded in AIF-deficient mice compared to WT mice (**A**, **B**). Hq/Y, harlequin hemizygous male mice.

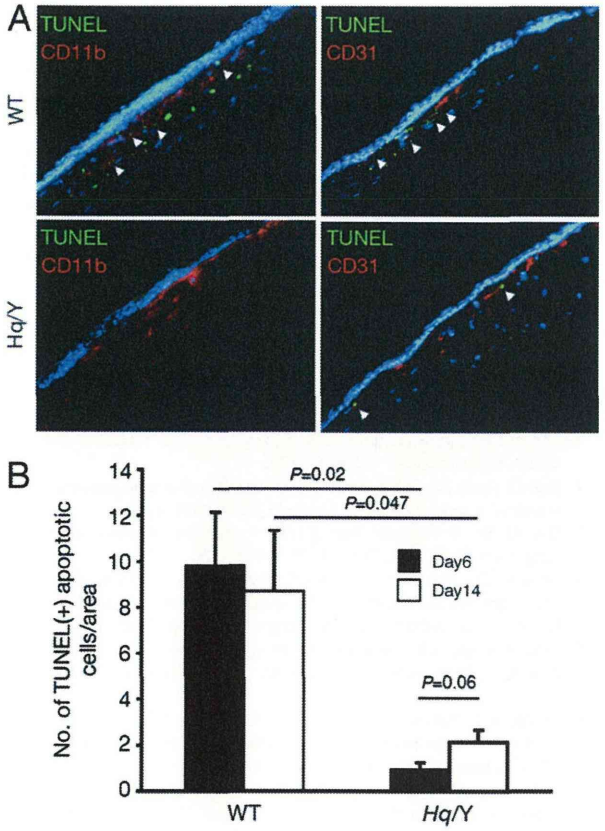

Figure 6. Immunohistochemistry for inflammatory and endothelial cells in the corneal micropocket assay. **A:** Immunostaining shows abundant infiltrated inflammatory cells (CD11b) and migrated neovascular endothelial cells (CD31) in AIF-deficient mice compared to WT mice. **B:** More TUNEL$^+$ apoptotic cells are observed in WT mice than in AIF-deficient mice. TUNEL$^+$ apoptotic cells had a trend to decrease on day 14 (late) in WT mice. In contrast, apoptotic cells had a trend to increase on day 14 (late) in AIF-deficient mice. Hq/Y, harlequin hemizygous male mice.

test the hypothesis that macrophages from AIF-deficient mice are resistant to apoptotic stimuli, we examined primary macrophage culture from Hq and WT mice. Peritoneal macrophages were collected and cultured with or without starvation. TUNEL$^+$ apoptotic macrophage increased after starvation, and AIF translocation from the cytosol into the nuclei were noted in these cells undergoing apoptosis (Figure 7). AIF deficiency diminished AIF translocation and protected macrophages from apoptotic cell death.

Discussion

AIF deficiency substantially expanded and prolonged formation of neovascularization, and retarded regression of neovascularization in both laser injury CNV- and VEGF-induced corneal neovascularization models. Furthermore, both anatomical and functional metrics of CNV (flat mount analysis and fluorescein angiography) supported the notion that AIF deficiency leads to more robust and larger neovascularization. We have reported that laser photocoagulation incites inflammation, leading to endothelial upregulation of intercellular adhesion molecule-1, which binds to CD18, mediating firm leukocyte-endothelial adhesion and transmigration.[34] Laser photocoagulation leads to production of VEGF by retinal pigment epithelial cells,[20,39] stimulating proliferation of adjacent choroidal vascular endothelium and upregulation of intercellular adhesion molecule-1 expression on endothelium.[40] Circulating leukocytes, which migrate in response to VEGF, also release VEGF, amplifying the locally produced VEGF response as they bind to the endothelium. In addition, leukocyte-derived cytokines can stimulate retinal pigment epithelial cells and fibroblasts to express VEGF,[41,42] as well as the chemotaxins IL-8, monocyte chemotactic protein-1,[43] metalloproteinases[44] and intercellular adhesion molecule-1.[45] These observations are consistent with our findings that AIF deficiency protected macrophages and neovascular endothelial cells from apoptosis, result in accumulation and prolongation of inflammatory macrophages and neovascular endothelial cells at the site of the developing neovascularization.

Macrophages have been shown to exhibit distinct functions during injury and repair, especially in neovascularization. We have reported that macrophages are

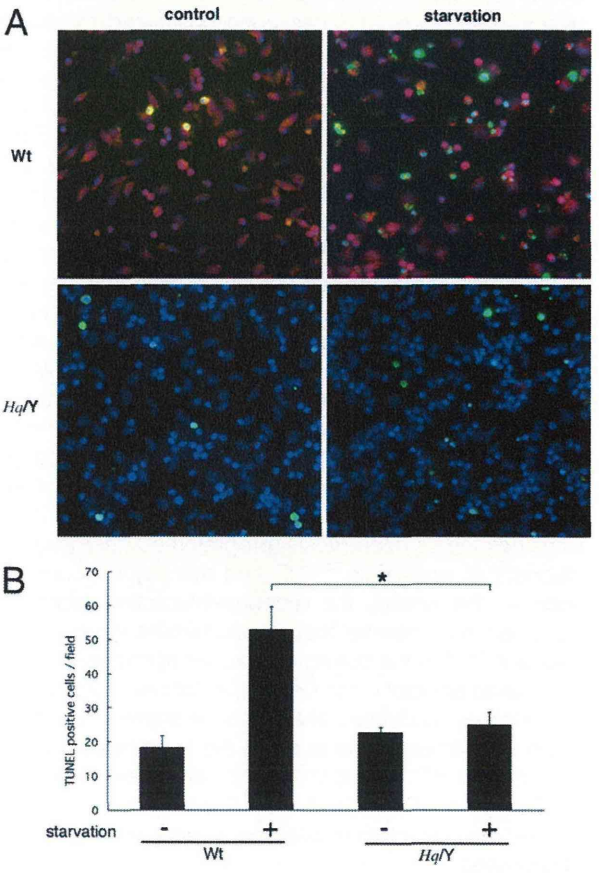

Figure 7. Peritoneal macrophage culture under starvation. Macrophages were collected from the peritoneal space and cultured using serum-free medium. **A:** WT mice show cytosolic (normal) and nuclear (apoptotic) staining for AIF, whereas AIF-deficient mice show no staining. **B:** TUNEL$^+$ apoptotic macrophages increase after 24 hours of starvation in WT mice. In contrast, macrophages from AIF-deficient mice are resistant to starvation. *$P < 0.05$. Hq/Y, harlequin hemizygous male mice.